nature climate change

SUPPLEMENTARY INFORMATION

DOI: 10.1038/NCLIMATE3322

In the format provided by the authors and unedited.

Global risk of deadly heat

Camilo Mora[1]*, Bénédicte Dousset[2], Iain R. Caldwell[3], Farrah E. Powell[1], Rollan C. Geronimo[1], Coral R. Bielecki[4], Chelsie W. W. Counsell[3], Bonnie S. Dietrich[5], Emily T. Johnston[4], Leo V. Louis[4], Matthew P. Lucas[6], Marie M. McKenzie[1], Alessandra G. Shea[1], Han Tseng[1], Thomas W. Giambelluca[1], Lisa R. Leon[7], Ed Hawkins[8] and Clay Trauernicht[6]

[1]Department of Geography, University of Hawai'i at Mānoa, Honolulu, Hawai'i 96822, USA. [2]Hawai'i Institute of Geophysics and Planetology, University of Hawai'i at Mānoa, Honolulu, Hawai'i 96822, USA. [3]Hawai'i Institute of Marine Biology, University of Hawai'i at Mānoa, Kāne'ohe, Hawai'i 96744, USA. [4]Department of Botany, University of Hawai'i at Mānoa, Honolulu, Hawai'i 96822, USA. [5]Department of Plant and Environmental Protection Sciences, University of Hawai'i at Mānoa, Honolulu, Hawai'i 96822, USA. [6]Department of Natural Resources and Environmental Management, University of Hawai'i at Mānoa, Honolulu, Hawai'i 96822, USA. [7]Thermal and Mountain Medicine Division, U.S. Army Research Institute of Environmental Medicine, Natick, Massachusetts 01760, USA. [8]National Centre for Atmospheric Science, Department of Meteorology, University of Reading, Reading, Berkshire RG6 6BB, UK. *e-mail: cmora@hawaii.edu

Supplementary Table 1. Earth System Models analyzed (Coupled Model Intercomparison Project Phase 5).

CENTER	COUNTRY	MODEL	Historical	RCP2.6	RCP4.5	RCP8.5
Commonwealth Scientific and Industrial Research Organization and Bureau of Meteorology	Australia	Access1.3	✔	-	✔	✔
Beijing Climate Center, China Meteorological Administration	China	BCC-CSM1.1	✔	✔	✔	✔
		BCC-CSM1.1(m)	✔	✔	✔	✔
College of Global Change and Earth System Science, Beijing Normal University	China	BNU-ESM	✔	✔	✔	✔
Canadian Centre for Climate Modelling and Analysis	Canada	CanESM2	✔	✔	✔	✔
Centre National de Recherches Meteorologiques / Centre Europeen de Recherche et Formation Avancees en Calcul Scientifique	France	CNRM-CM5	✔	✔	✔	✔
Commonwealth Scientific and Industrial Research Organization with Queensland Climate Change Centre of Excellence	Australia	CSIRO-Mk3.6.0	✔	✔	✔	✔
Met Office Hadley Centre	UK	HadGEM2-CC	✔	-	✔	✔
Met Office Hadley Centre (additional HadGEM2-ES realizations contributed by Instituto Nacional de Pesquisas Espaciais)	UK	HadGEM2-ES	✔	✔	✔	✔
Institute for Numerical Mathematics	Russia	INM-CM4	✔	-	✔	✔
Institute Pierre-Simon Laplace	France	IPSL-CM5A-LR	✔	✔	✔	✔
		IPSL-CM5A-MR	✔	✔	✔	✔
		IPSL-CM5B-LR	✔	-	✔	✔
Atmosphere and Ocean Research Institute (The University of Tokyo), National Institute for Environmental Studies, and Japan Agency for Marine-Earth Science and Technology	Japan	MIROC4h *	✔	-	✔	-
		MIROC5	✔	✔	✔	✔
Japan Agency for Marine-Earth Science and Technology, Atmosphere and Ocean Research Institute (The University of Tokyo), and National Institute for Environmental Studies	Japan	MIROC-ESM	✔	✔	✔	✔
		MIROC-ESM-CHEM	✔	✔	✔	✔
Meteorological Research Institute	Japan	MRI-CGCM3	✔	✔	✔	✔
		MRI-ESM1	✔	-	-	✔
Norwegian Climate Centre	Norway	NorESM1-M	✔	✔	✔	✔

List of models used in this study. We only considered models that provided the complete series of data from 1950 to 2100 for surface downwelling shortwave radiation (rsds), daily-mean near-surface wind speed (sfcWind), near-surface relative humidity (rhs), daily mean near-surface air temperature (tas), daily minimum near-surface air temperature (tasmin) and daily maximum near-surface air temperature (tasmax).
* Projection ends in 2035.

Fig. S1. Characterization of climatic conditions during heat lethal events. For the place and time of each lethal heat, we calculated 16 climatic variables described below.

1. Mean daily temperature during the days of the event (^{o}C).
2. Mean minimum daily temperature during the days of the event (^{o}C).
3. Mean maximum daily temperature during the days of the event (^{o}C).
4. Mean daily relative humidity during the days of the event (%).
5. Mean daily wind speed during the days of the event (m/s).
6. Mean daily solar radiation during the days of the event (watts/m^2).
7. Cumulative number of degrees Celsius above the 90th percentile during the days of the event, using mean daily temperature (heating degree days, ^{o}C).
8. Same as #7 but using minimum daily temperature.
9. Same as #7 but using maximum daily temperature.
10. Cumulative humidity above the 90th humidity percentile for the period of the heat event.
11. Cumulative wind speed above the 90th wind speed percentile for the period of the heat event.
12. Cumulative solar radiation above the 90th radiation percentile for the period of the heat event.
13. Duration (number of days of the event).
14. Intensity (the largest difference between the mean daily temperature and the 90th temperature percentile, ^{o}C).
15. Time to peak of summer (i.e., number of days between the time of the event and the hottest day in the climatology, in days). Heat episodes that occur close to the peak of the summer are assumed to be dangerous because, in such cases, temperature can exceed the maximum adaptability gained historically during the hottest times of the summer.
16. Absolute temperature change (mean difference between the maximum and minimum daily temperatures during the heat event, ^{o}C). Heat event with small absolute thermal change could be dangerous because high temperatures persisting overnight preclude physiological recovery.

Fig. S2. Support Vector Machine models for pairs of variables analyzed in this study. A total of 16 variables were used in this study to discriminate the climate conditions during days that were lethal and not. Below is a subset of pair-wise models. The accuracy of each SVM is shown inside the plots. Red lines are the SVM thresholds that best separate lethal and non-lethal heat events; shaded red areas indicate the side of the threshold where conditions are classified as deadly. Black points indicate conditions of documented lethal heat events. Red to green gradient indicates the density of non-lethal events. The classification accuracy for all possible combinations of all 16 variables is shown in Fig. S3.

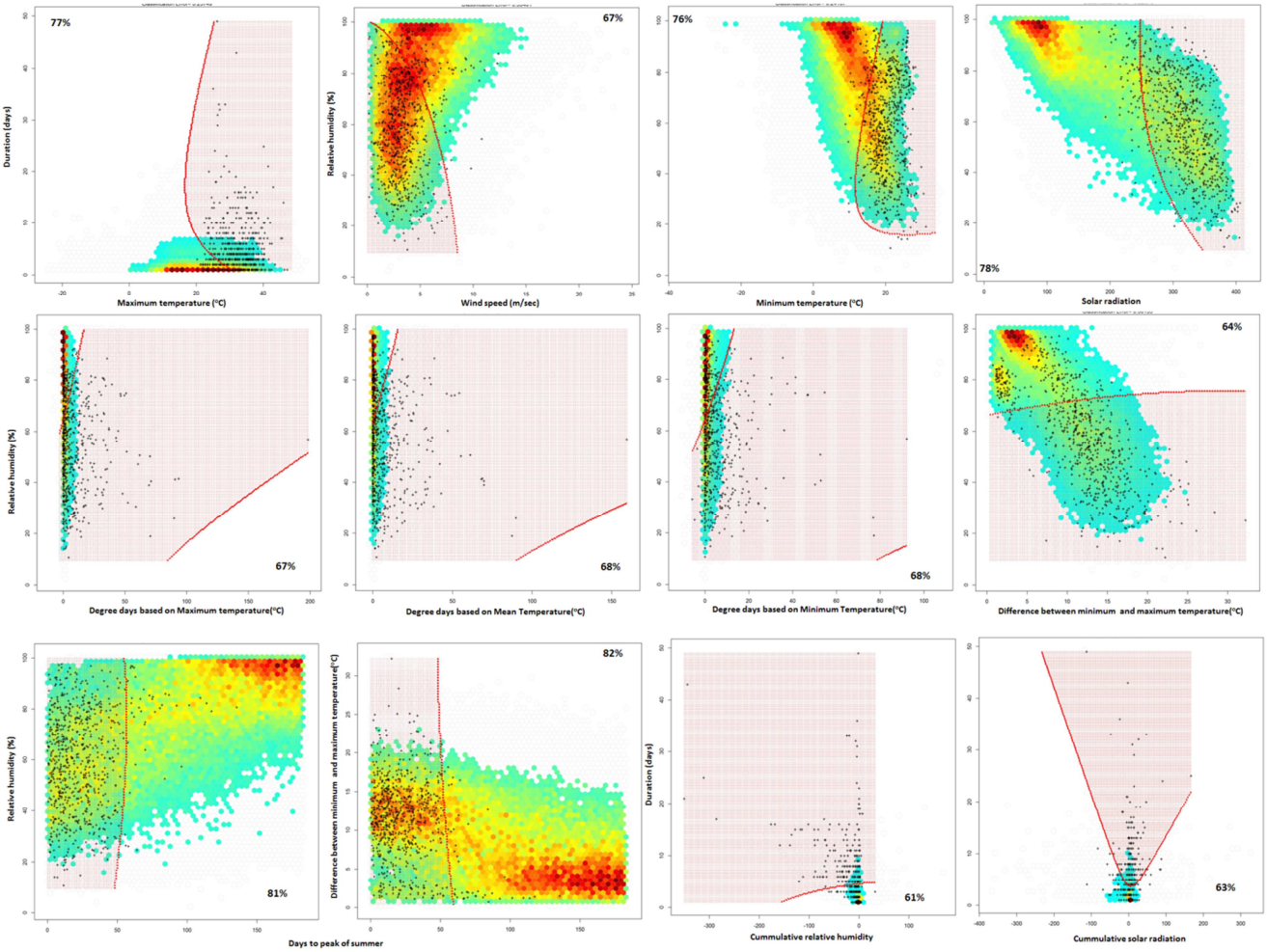

Fig. S3. Improvements in SVM accuracy (i.e., classification error) with increases in the number of variables considered. Black points represent each of the 65,535 potential SVM models resulting from all possible combinations of the 16 climatic variables used in this study. A model with mean daily surface air temperature and mean daily relative humidity yielded an accuracy of 83% (horizontal line in the plot below), which was the highest accuracy of any two pairs of variables. Less parsimonious models increased accuracy only minimally, with the model including all 16 variables improving accuracy by only 3%.

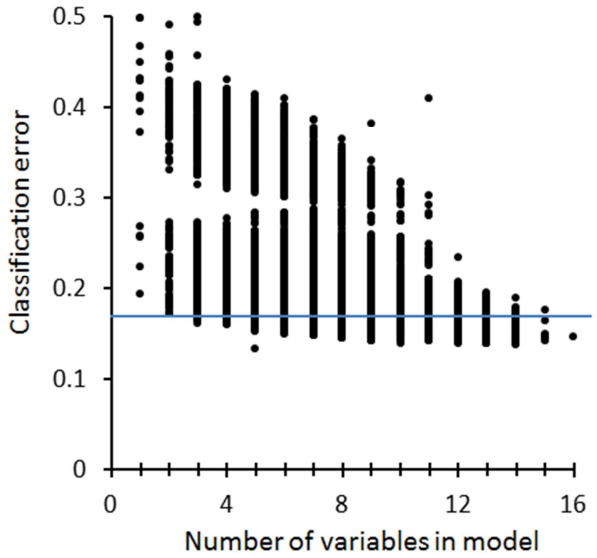

Fig. S4. Current and projected changes in deadly climatic conditions. Extended results of Fig. 2. Plots show the area of the planet and global population exposed to various numbers of days surpassing the deadly threshold.

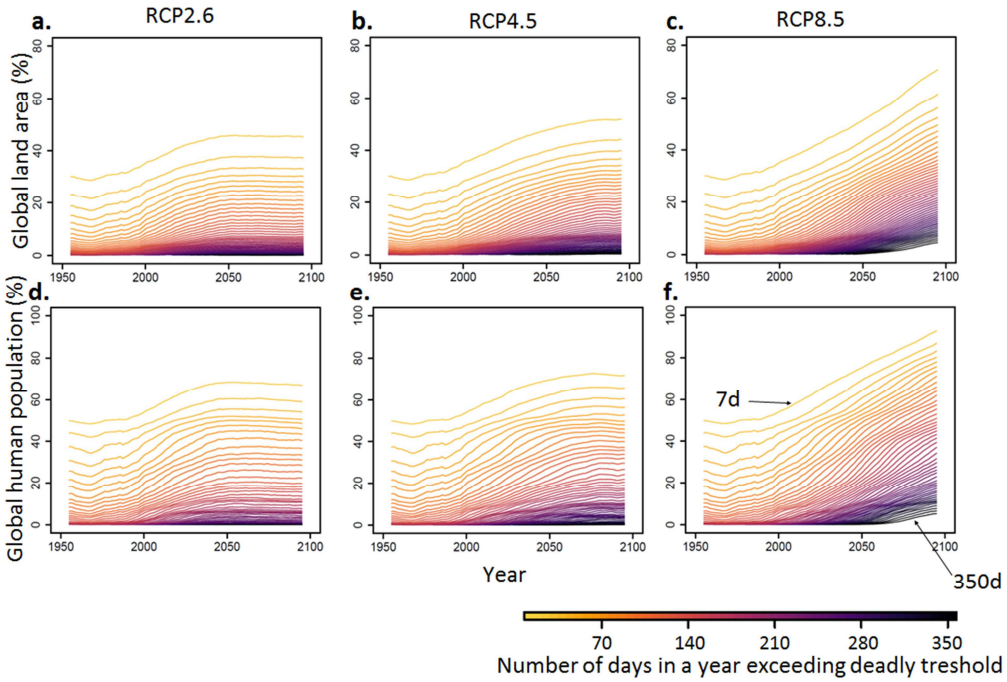

Fig. S5. Spatio-temporal changes in deadly climatic conditions. Extended results of Fig. 5 for each of the RCPs.

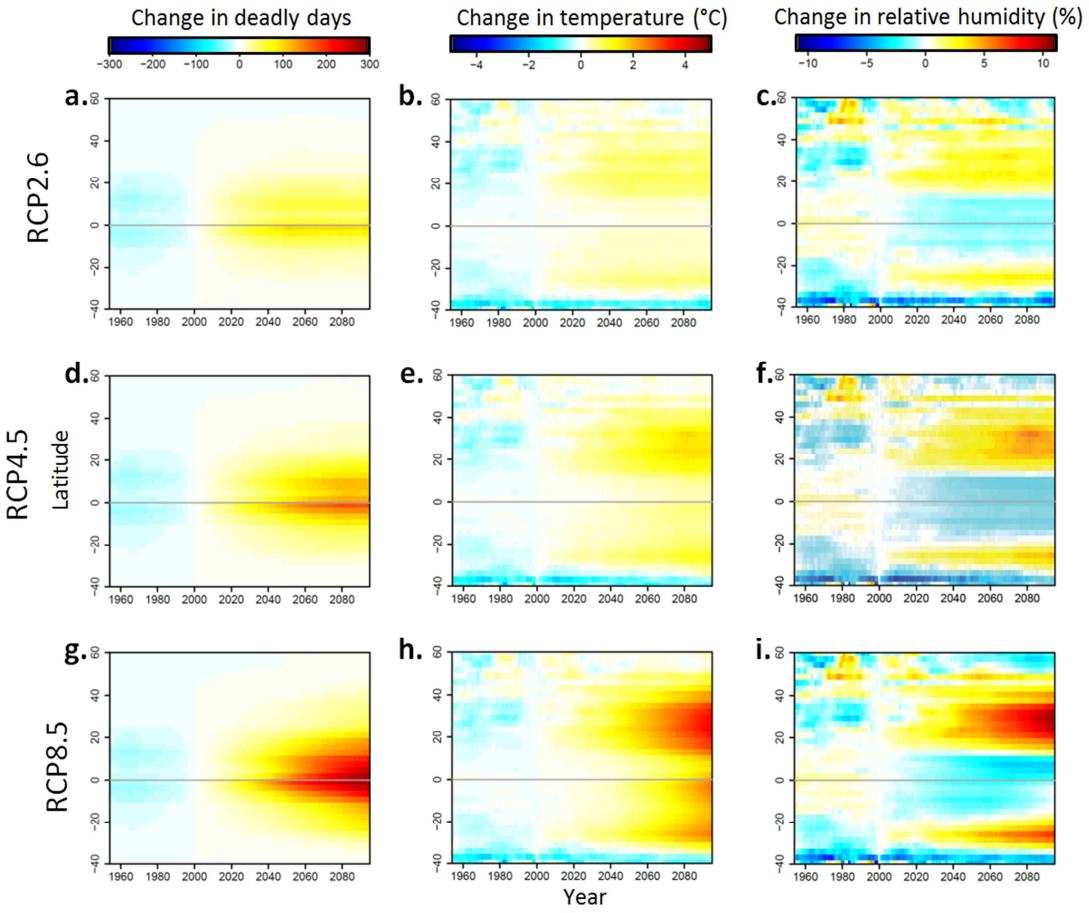

Fig. S6. Proximity of climatic conditions to the deadly threshold by latitude under different RCPs. Distribution of the percentage of days in a given year (i.e., color gradients), at each latitude, as a function of their temperature (**a-d**), relative humidity (**e-h**), and distance to the deadly threshold (**i-l**). Displayed here are the last year in the historical experiment (i.e., 2005); (**a**) and the year 2100 under RCP 2.6 (**b**), RCP 4.5 (**c**) and RCP 8.5. Illustrations are based on a randomly chosen model (i.e., CSIRO-Mk3-6-0). Vertical black lines are shown as a guide for comparison among plots.

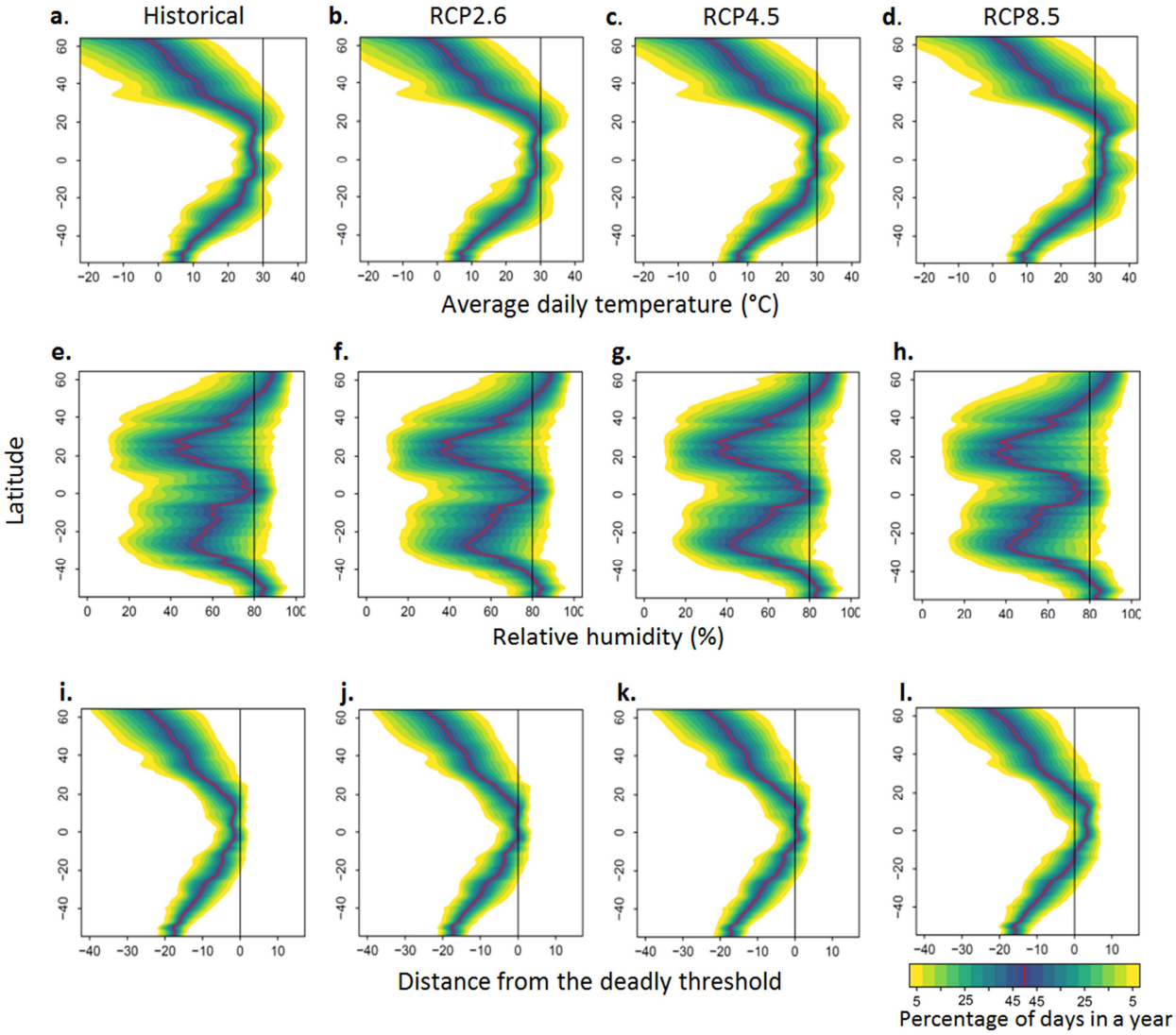

Fig. S7. Possible mechanisms for large scale variations in the conditions of deadly days. Over time the number of deadly days increased most substantially towards the tropics (**a**) despite the less extreme warming there (**b**). Such less extreme warming, however, is accompanied by increases in relative humidity in tropical areas (**c**). Tropical areas have predominantly higher soil moisture in contrast to dry mid-latitudes (**d**). Soil moisture affects the partitioning of energy fluxes (e.g., Bowen ratio: sensible heat/latent heat, **f**), with the lack of moisture availability in dry areas increasing sensible heat flux, thus amplifying extreme temperatures (**i**). All plots are based on RCP8.5. Data in plots **f-i** are for the year 2100. Change in temperature in plot **i**, is the absolute difference between 2005 and 2100.

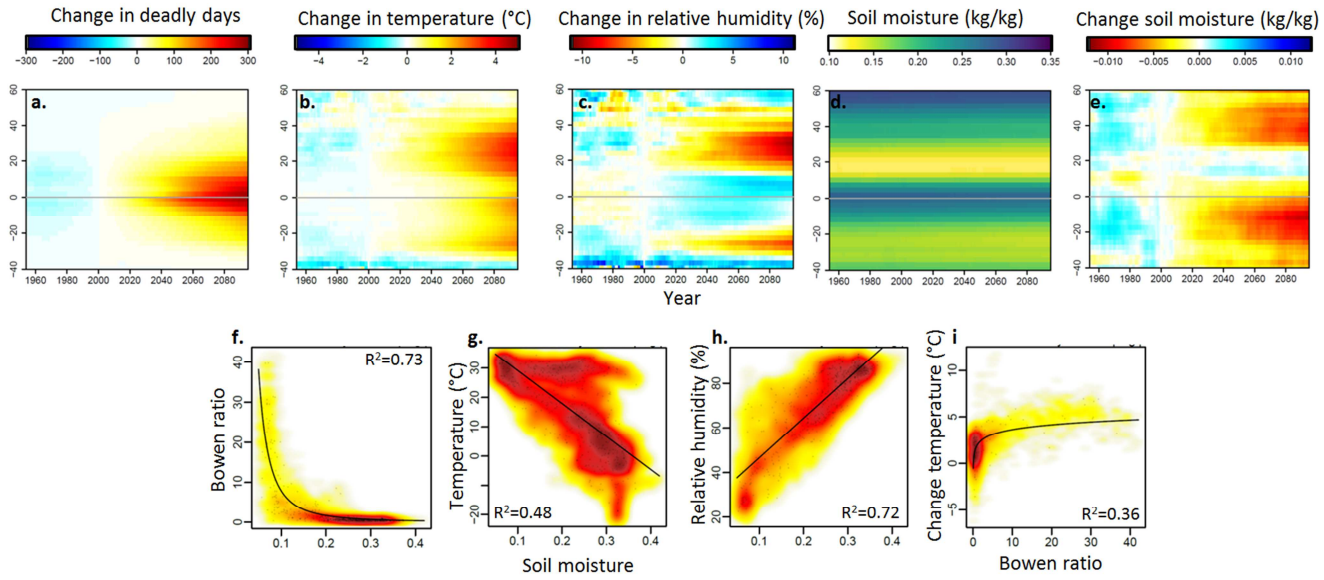

Fig. S8. Effect of climatology bias in Earth System Models in predicting deadly climates. Climatic projections of Earth System Models can be offset from actual climatic values due to variability in the initial parameters used in the model. This bias can affect results based on threshold analyses that rely on absolute values. For instance, consider a model with a 2°C negative bias (i.e., the model simulates 2°C colder than it actually is) and the objective is to assess whether temperature of a given place exceeds a 32°C threshold. If this model simulates a 31°C temperature, the nominal data will indicate that temperature does not exceed the 32°C threshold. However, if the 2°C bias in the model is accounted for, then the expected temperature will be 33°C, which does exceed the 32°C threshold. To assess the effect of climatological biases in Earth System Models, we ran the SVM model based on mean daily temperature and relative humidity with the nominal data from the Earth System Models, and with data that subtracted any bias in the climatology of the two variables. For each variable in the CMIP5 models and NCEP-DOE Reanalysis data from 1980 to 2005, we calculated their climatology (average value) for every global cell for any given day of the year plus and minus two days (a five day window centered in the given day of the year). The climatology from the Earth System Model was subtracted from the climatology of reanalysis data and this "bias" was added to the projected variables for the given cell and time of the year for that given model. In the case of relative humidity, any bias-corrected values above 100% were set to 100%. The results from all CMIP5 models with raw and bias-corrected data were grouped and averaged to create a multi-model average of each type of data. The plots below show the number of days per year above the SVM threshold with the two sources of data for the year 2005 (**a**) , and coefficient of determination (R^2) for every individual year from 1980 to 2005 (**b**). The high similarity between the nominal data and the bias corrected data is probably explained by the fact that the use of a multimodel average can even up biases among models, although it has also been shown that model errors are reduced in analyses that combine temperature and relative humidity (Fig. S10).

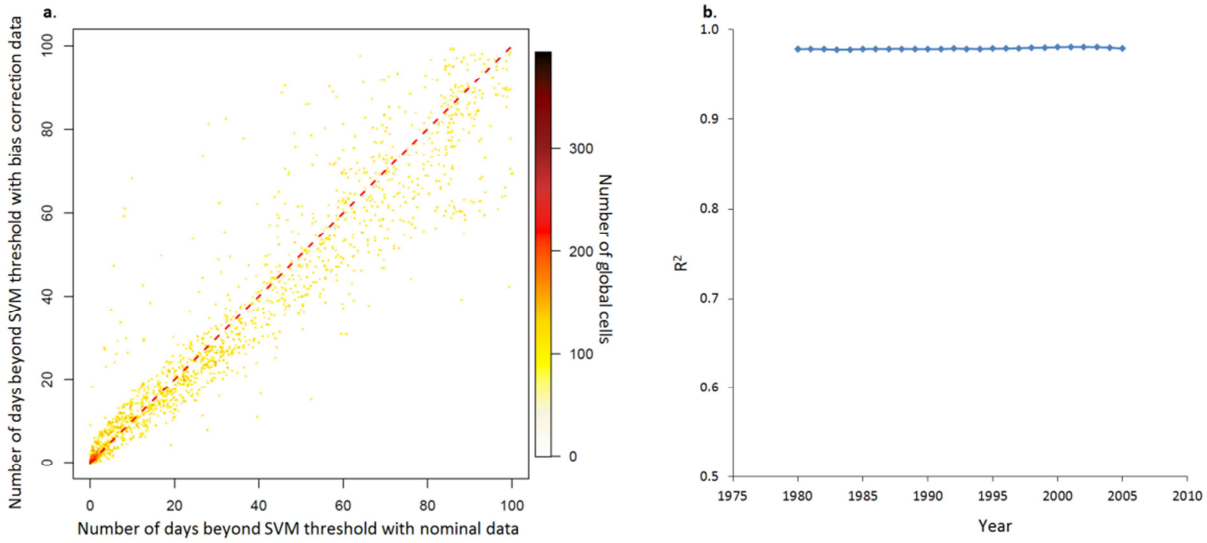

Fig. S9. Comparison of deadly heat anomalies from NCEP-DOE Reanalysis data with individual Earth System Models and their multimodel median. Comparisons of the cumulative number of days beyond the deadly SVM threshold (**a**), and temperature (**b**) and relative humidity (**c**) during those days between each CMIP5 Earth System Model and their multimodel median to the same attributes predicted from the NCEP-DOE Reanalysis data from 1980 to 2005 (the common time frame for both data sources). The Taylor diagrams below compare NCEP-DOE Reanalysis data with CMIP5 model simulations and summarize three different metrics of similitude: correlation (curved axis), ratio of the standard deviations (x and y axes), and root mean squared error (blue arcs). Blue points indicate perfect fit, red points indicate the multimodel average, and black points indicate the comparison of each Earth System Model to the NCEP-DOE Reanalysis data. The closer a red or black point is to the blue point, the better the fit between reanalysis and simulated data.

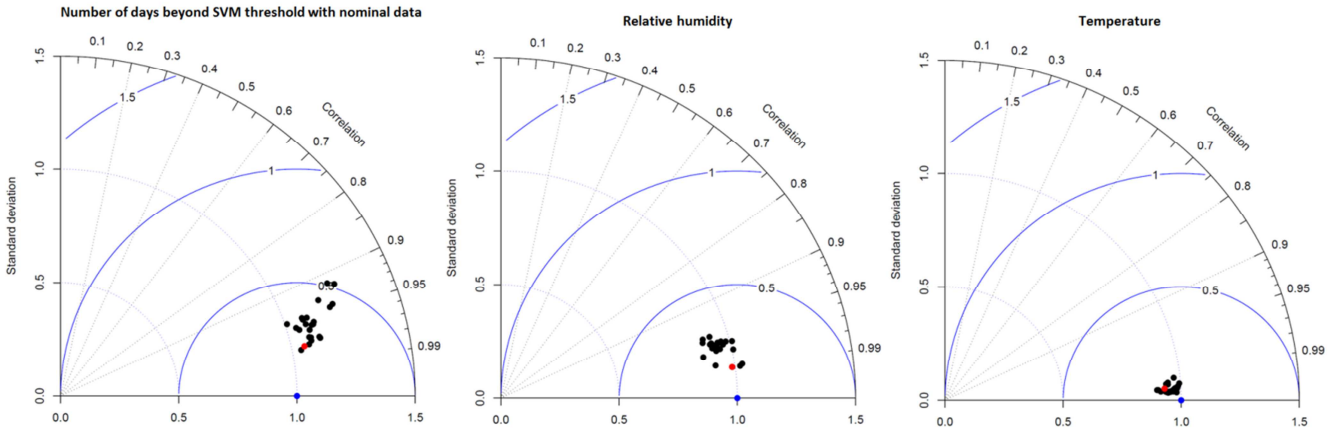

Fig. S10. Potential effects of projection errors in reported trends. Two key sources of error in our analysis are related to the "accuracy" and "precision" with which data from Earth System Model predict the occurrence of deadly climatic conditions. Accuracy can be broadly defined as the extent to which a measurement resembles the true value and precision as the variability among replicated measurements. To quantify accuracy, for each land cell, we calculated the difference between the number of deadly days in a year predicted using the re-analysis data minus the CMIP5 multimodel median for the year 2005. To quantify precision, at each time step for each land cell, we quantified the standard deviation among CMIP5 models in their predictions of the number of deadly days in a year, and divided that value by the multimodel mean to calculate the coefficient of variance (CV). To assess the extent to which these two sources of error affect our results, for each land cell, we subtracted the accuracy error from the multimodel median prediction of the number of deadly days (red-lines in the plots below); independently, we also removed any cell with a CV large than 100% (blue lines in the plots below) and in a third test, we removed any cell with CVs larger than 100% and for those cells that remained we subtracted the error in accuracy (green lines in plots below). From the resulting data, we calculated the area of the planet and the percent of the global population exposed to more than 20 deadly days in a year as in Fig. 2 of the paper. The analyses were repeated independently for the nominal data and the data correcting for each model's mean climatology bias (see Fig. S8). As noted in the figures below, precision among Earth System models added the largest error in our analysis but even when combined with the errors in accuracy and using nominal or climatology bias correction data, such errors were insufficient to modify the general trends reported here. Several factors may explain this. First, general trends are based on a multimodel median ensemble. Second, results are based on variables that are relatively well predicted by Earth System Models (Fig. S9). Finally, our approach combines temperature and humidity, which are two variables that have been found to yield robust projections when used in combination, as their causal interrelation considerably reduces uncertainties (Fischer & Knutti 2013).

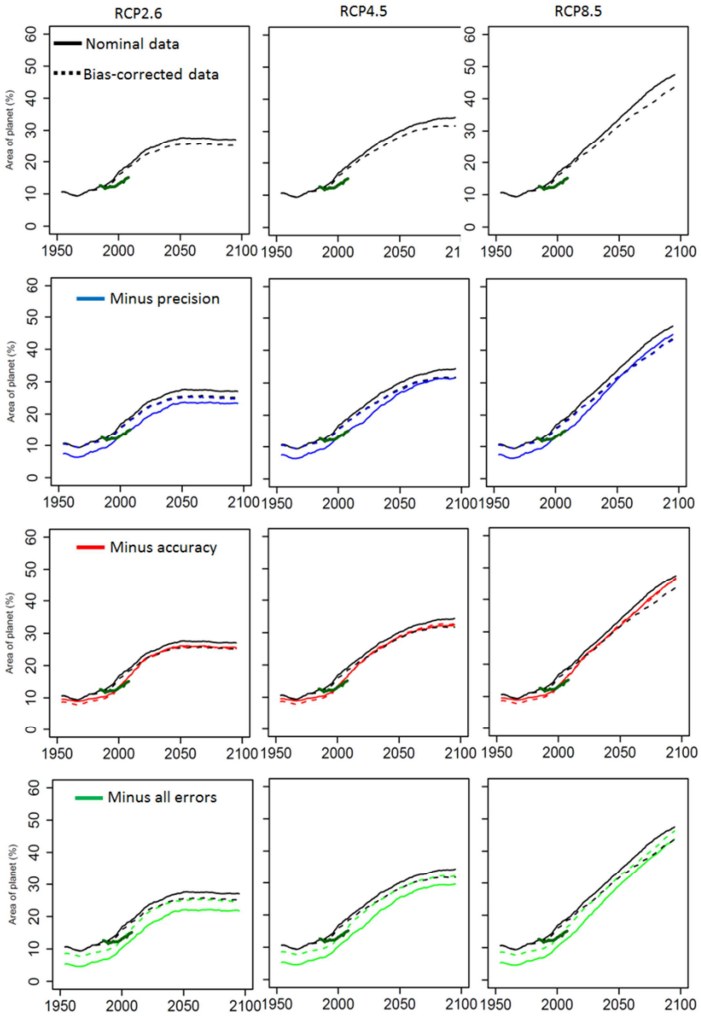

Cont. Fig. S10. Accounting for errors in human population data. Note that the fraction of the world's human population exposed to deadly climates has a slight "jump" around the year 2005, which is related to the shift in the human population databases used. The CIESIN database was used for any climatic projection prior to 2005, whereas the SSP human population projections were paired with the different RCPs after 2006 (see methods).

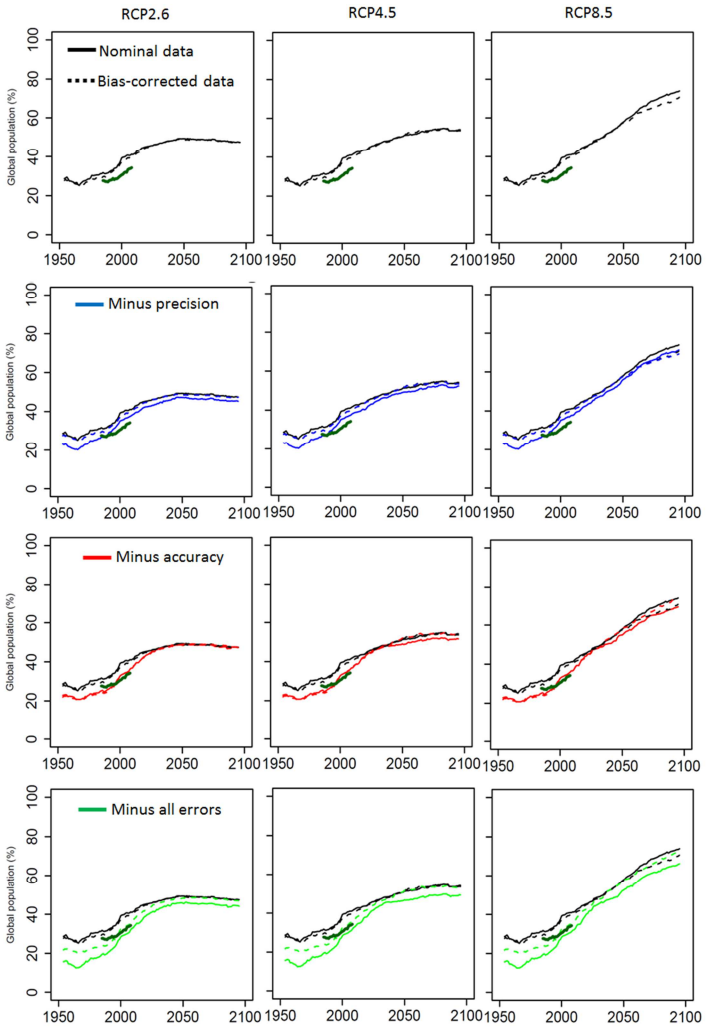

General considerations: The "accuracy" correction improved the similarity between the re-analysis and the CMIP5 data (compare red vs. dark green lines) in contrast to the direct bias correction in the climatology of temperature and relative humidity (compare straight vs. dashed lines). This suggest that the ~3% mismatch in the area of the planet (~6.4% in global population) between the reanalysis and the multimodel median is due to the treatment of the climatological bias of two variables that are related and are not independent as treated in our bias-correction test and that the "accuracy" correction is more appropriate in our case. In any case, the error in accuracy does not revert the reported trends (compare solid light-green vs. black lines).

The "accuracy" correction caused a variable effect over time despite the fact that "accuracy" is a constant. This happens because accuracy was estimated spatially (i.e., each pixel has a bias in the number of days) that is added to the simulated deadly days for that pixel, and then aggregated globally over time to generate the trend lines above. So, it is not always the case that accounting for accuracy in a given pixel will add or subtract enough deadly days in a year for that pixel to be counted in the global results shown in the trends. This variability along the accuracy trend (red lines) is larger in the human population projections, because locations (cells) affected will have different numbers of people living within them.

E. Fischer, R. Knutti, Robust projections of combined humidity and temperature extremes. Nat. Clim. Change 3, 126 (2013)